International Journal of Nanomedicine

Dovepress
open access to scientific and medical research

Open Access Full Text Article

ORIGINAL RESEARCH

Development of Paeonol Liposomes: Design, Optimization, in vitro and in vivo Evaluation

Shan Huang[1], Bingtao Zhai[1], Yu Fan[2], Jing Sun[1], Jiangxue Cheng[1], Junbo Zou[1], Xiaofei Zhang[1], Yajun Shi[1], Dongyan Guo[1]

[1]Shaanxi Province Key Laboratory of New Drugs and Chinese Medicine Foundation Research, College of Pharmacy, Shaanxi University of Chinese Medicine, Xianyang, 712046, People's Republic of China; [2]School of Basic Medicine, Shaanxi University of Chinese Medicine, Xianyang, 712046, People's Republic of China

Correspondence: Dongyan Guo, Tel +86-029-38185180, Email xmc2051080@163.com

Background: Ulcerative colitis (UC) is one of the intractable diseases recognized by the World Health Organization, and paeonol has been proven to have therapeutic effects. However, the low solubility of paeonol limits its clinical application. To prepare and optimize paeonol liposome, study its absorption mechanism and the anti-inflammatory activity in vitro and in vivo, in order to provide experimental basis for the further development of paeonol into an anti-inflammatory drug in the future.

Methods: Paeonol loaded liposomes were prepared and optimized by thin film dispersion-ultrasonic method. The absorption mechanism of paeonol-loaded liposomes was studied by pharmacokinetics, in situ single-pass intestinal perfusion and Caco-2 cell monolayer model, the anti-inflammatory activity was studied in a mouse ulcerative model.

Results: Box-Behnken response surface methodology permits to screen the best formulations. The structural and morphological characterization showed that paeonol was entrapped inside the bilayer in liposomes. Pharmacokinetic studies found that the AUC_{0-t} of Pae-Lips was 2.78 times than that of paeonol suspension, indicating that Pae-Lips significantly improved the absorption of paeonol. In situ single intestinal perfusion and Caco-2 monolayer cell model results showed that paeonol was passively transported and absorbed, and was the substrate of P-gp, MRP2 and BCRP, and the Papp value of Pae-Lips was significantly higher than that of paeonol. In vitro and in vivo anti-inflammatory experiments showed that compared with paeonol, Pae-Lips exhibited excellent anti-inflammatory activity.

Conclusion: In this study, Pae-Lips were successfully prepared to improve the oral absorption of paeonol. Absorption may involve passive diffusion and efflux transporters. Moreover, Pae-Lips have excellent anti-inflammatory activity in vitro and in vivo, which preliminarily clarifies the feasibility of further development of Pae-Lips into oral anti-inflammatory drugs.

Keywords: paeonol liposomes, intestinal absorption, Caco-2 monolayer cell model, absorption mechanism, anti-inflammatory activity

Introduction

Ulcerative colitis (UC), a common chronic inflammatory bowel disease, the main clinical symptoms contain diarrhea, abdominal pain, and bloody stools.[1,2] It is one of the most intractable diseases recognized by the World Health Organization.[3] In addition to surgical resection, currently commonly used treatment drugs include salicylic acid, glucocorticoids, immunosuppressive agents, and so on.[4] However, in the long run, they are accompanied by adverse reactions such as kidney and liver side effects, leukopenia and other adverse reactions.[5,6] Therefore, the development of innovative and effective drugs from natural resources is particularly significant for reducing side effects and improving treatment effects. In recent years, traditional Chinese medicine has played an increasingly important role in UC treatment due to its multi-target and multi-component characteristics.[7–9]

In Chinese medicine, Moutan Cortex, the root bark of Paeonolonia suffruticosa Andrews (Paeonoloniaceae), has antipyretic, analgesic and anti-inflammatory effects.[10] Paeonol, 2'-hydroxy-4'-methoxyacetophenone, is the main phenolic component of Cortex Moutan, which has a wide range of pharmacological activities, such as anti-inflammatory activity,[11] antibacterial activity,[12] anti-allergic activity,[13] anti-tumor activity,[14] and so on. Among them, the anti-inflammatory effect is

Received: 23 February 2022
Accepted: 7 September 2022
Published: 25 October 2022

particularly prominent.[15] Studies have shown that paeonol can block the inflammatory response of BV-2 and RAW264.7 cells stimulated by LPS by regulating the mitogen-activated protein kinase (MAPK) and nuclear factor-κB (NF-κB) signal pathways.[16] In addition, DSS induces mice in the UC model, paeonol and its metabolites exert anti-inflammatory and antioxidant effects by blocking the MAPK/ERK/p38 signaling pathway.[17] However, paeonol has low oral bioavailability, low water solubility, and poor stability, which severely restrict its clinical application.[18,19] Generally speaking, factors that affect drug absorption include physiological factors, drug factors, and formulation and dosage form factors. Therefore, it is necessary to develop suitable formulations to improve the bioavailability of paeonol. In the past, different formulations of paeonol have been studied to improve its bioavailability.[20,21]

Liposomes are mainly composed of phospholipid bilayer membranes, containing hydrophilic and lipophilic molecules, with a cell-like structure similar to biological membranes.[22] Many advantages of liposomes were already verified, such as targeting, low toxicity, biocompatibility, and long-term sustained release.[23,24] Some studies have reported that liposomes are not suitable for oral administration, but new findings in the field underscore their effectiveness, especially when phospholipids are used in high concentrations.[25,26] Studies have shown that liposome entrapment have the abilities to improve the dissolution and bioavailability of drugs.[27–29] Therefore, in this study, the Box-Behnken effect surface method was used to optimize the paeonol liposomes, and the overall absorption characteristics were investigated by pharmacokinetic experiments, which showed that the liposomes significantly enhanced the absorption of paeonol. Then the specific mechanism by which the liposomes could enhance the absorption of paeonol was further investigated by in situ single-pass intestinal perfusion experiments and Caco-2 monolayer cell model. Finally, the effects of paeonol and Pae-Lips on LPS-stimulated RAW264.7 inflammation and on DSS-induced UC were investigated, and liposomes were found to enhance the anti-inflammatory effects of paeonol.

Materials and Methods

Materials

Paeonol was purchased from Xi'an Deshengyuan Biotechnology Co., Ltd. (purity 99%, Xi'an, China). Soybean phosphatidylcholine (SPC, purity >98%) and cholesterol (CHOL, purity >98%) were purchased from Macleans Biochemical Co., Ltd. (Shanghai, China). Cell culture material trypsin-0.25% EDTA was purchased from Beijing Sun Technology Co., Ltd. (Beijing, China), αMDM medium, DMEM medium, Hanks Buffer (HBSS) and penicillin-(100×) were purchased from Boster, dimethyl sulfoxide (DMSO) was purchased from Sigma, transwell chambers and 12-well Millicell plates were purchased from Millipol, USA. Verapamil (Ver), Indomethacin (Indo), Reserpine (Res) (purity >98%) came from Shanghai Yuanye Biotechnology Co., Ltd (Shanghai, China). Dextran Sulfate (DSS) was provided by MP Biomedicals LLC. The mouse interleukin 6 (IL-6), anti-tumor necrosis factor alpha (TNF-α) and interleukin 10 (IL-10,) ELISA kits for cells were purchased from Jiangsu Enzyme Immunology Co., Ltd., IL-6, IL-10 and TNF-α (A28210345) for animals were purchased from Jiangsu Enzyme Immunology Co., Ltd.

Animals and Cells

Sprague-Dawley male rats, body weight (250 ± 20) g; Male Balb/c mice (24 ± 5) g, the above animals were purchased from Chengdu Dashuo Experimental Animal Co., Ltd., animal production license number SCXK (chuan) 2020–030. All animal experiments were approved by the Experimental Ethics Committee of Shaanxi University of Traditional Chinese Medicine. All animal experiments followed the regulations of Shaanxi University of Traditional Chinese Medicine on the management methods and use of experimental animals, and all complied with the 3R principle.

Caco-2 cells were purchased from Qishi Biotechnology Co., Ltd. (Wuxi, China); RAW264.7 cells were purchased from Suzhou Meilum Biotechnology Co., Ltd. (Suzhou, China).

Formulation Preparation and Optimization

HPLC Analysis

The content of paeonol was measured by high performance liquid chromatography (1260, Agilent, USA). Chromatographic conditions: chromatographic column is HyPURITY C_{18} (250 mm × 4.6 mm, 5 μm), mobile phase is methanol and water 80:20

(v/v), volume flow rate 0.8 mL/min, the injection volume is 10 μL, and the column temperature is 30°C. Paeonol was detected at a wavelength of 254 nm.

Preparation of Pae-Lips

The film dispersion-ultrasonic method was used to prepare Pae-Lips. Weigh the paeonol (30 mg), CHOL (33.3 mg) and SPC (200 mg), add absolute ethanol (20 mL) to dissolve it, and rotate evaporation at 45°C under an evaporator (N-1200B, JEOL, Japan) until it became a transparent film. Then add PBS (10 mL) to hydrate until there are no insolubles in the solution, ultrasonic treatment, finally the suspension is passed through 0.22 μm microporous membrane to form Pae-Lips.

Box–Behnken Effect Surface Method to Optimize Prescription

According to the results of the previous single-factor experiment, the Pae-Lips preparation process was optimized by the Box-Behnken effect surface method. Select factor A (SPC: CHOL, w/w), B (the concentration of paeonol, mg/mL) and C (pH of PBS) were treated as the impact factors, the entrapment efficiency (EE%) as the response value. The test results were analyzed by Design Expert 12.0. To resort to the Box-Behnken effect surface optimization experiment, the best prescription was obtained and verified by 3 parallel experiments.

Characterization of the Pae-Lips

Particle Size and Zeta Potential

The particle size (PS), polydispersity index (PDI) and Zeta potential of the Pae-Lips were measured with the particle size analyzer (ZS90, Malvern, UK).

EE% and Drug Load (DL%)

The EE% and DL% of Pae-Lips were determined by ultrafiltration centrifugation. In short, put 500 μL Pae-Lips in an ultrafiltration centrifuge tube, centrifuge at 4°C, 13,500 rpm for 30 min, flowed out liquid was collected and determined by HPLC, recorded as C_1, the total content of Pae-Lips was recorded as C. The EE% and DL% of Pae-Lips was calculated according to the following formulas:

$$EE\% = \frac{C - C_1}{C} \times 100\%$$

$$DL\% = \frac{W_0}{W} \times 100\%$$

W is the total drug mass; W_0 is the mass of paeonol in the paeonol loaded liposomes.

Transmission Electron Microscopy (TEM)

The morphology of Pae-Lips was characterized by a transmission electron microscope (JEM-1230, JEOL, Japan). The sample was negatively stained with 2% phosphotungstic acid on a copper mesh and dried at room temperature.

Differential Scanning Calorimetry (DSC) Analysis

The thermal properties of paeonol, CHOL, SPC, physical mixture (PM) and freeze-dried Pae-Lips powder were studied by DSC (Mettler Toledo TGA/DSC3+, Swiss Schwerzenbach). The temperature ranging from 10°C to 400°C was selected and the sample was thermally scanned at a heating rate of 5°C/min at a constant nitrogen flow rate.

X-Ray Diffraction (XRD)

The XRD pattern was obtained by using a Cu-K radiation source (40 kV 100 mA) advanced diffractometer (Bruker-AXS D8, Karlsruhe, Germany). The X-ray scan rate is 0.02°/s, and the range is from 10° to 70°.

FTIR Spectroscopy (FTIR)

FTIR spectra of paeonol, CHOL, SPC, PM, and Pae-Lips were obtained in an IR diffraction spectrophotometer (TENSOR-27, Bruker, Germany). The samples were scanned over the range 4000–400 cm^{-1}.

In vitro Drug Release

The release behavior of paeonol from paeonol suspension and Pae-Lips were measured using a dialysis method. In brief, 2 mL of the preparation (containing the same amount of paeonol) were placed in a dialysis bag and separately placed (containing 0.5% tween-80) in 60 mL of release medium PBS (pH 7.4), artificial gastric juice (SGF), and artificial intestinal fluid (SIF) incubate with shaking (37°C, 100 rpm). At designated intervals, 1 mL of sample was taken out for HPLC analysis, and the same volume of fresh medium was added. Calculate the cumulative drug release percentage P% according to the following formula:

$$P\% = \frac{(V \times C_n + \sum C_i \times V_s)}{Q_0} \times \%$$

C_n represents the paeonol concentration of the nth sampling point, C_i represents the concentration of each previous sampling point, V and Vs represent the release medium volume and sampling volume, respectively, and Q_0 represents the initial drug content.

Stability Study

The stability of Pae-Lips was estimated in SGF and SIF, 1 mL of Pae-Lips injected into 50 mL of medium and placed them on a 37°C shaker (65 rpm), the particle size and PDI were measured using NanoZetasizer at designated intervals.

The paeonol liposomes were placed at 4°C, 25°C and 40°C, respectively, and their particle size, EE% and Zeta potential were measured at a certain time point within 15 days to investigate their stability.

In vivo Pharmacokinetics Studies

Male Sprague-Dawley rats (250 ± 20 g) were randomly divided into two groups with 6 rats in each group. Fasting for 12 hours before administration, but free to drink water. The rats in the two groups were given oral paeonol suspension (dispersed in 0.5% CMC-Na, 100 mg/kg) and Pae-Lips (100 mg/kg). At 0.083, 0.167, 0.25, 0.5, 0.75, 1, 1.5, 2, 3, 4, 6, 8, 12 h after administration, about 1 mL of orbital blood was taken in heparinized test tube. All collected blood samples were centrifuged at 13,500 rpm and 4°C for 15 minutes, then the supernatant plasma samples were taken and frozen at −20°C for further analysis by HPLC.

In situ Single-Pass Intestinal Perfusion (SPIP)

Before the operation, the rats were fasted for about 12 hours and drunk freely. The rats weighing 250 ± 20g were anesthetized by intraperitoneal injection of 10% urethane, and the back position was fixed on the operating table Open the abdominal cavity about 4 cm along the midline of the abdomen, separate the duodenum, jejunum, ileum and colon about 10 cm, respectively. Carefully insert the silicone tube and ligate it. Rinse the intestinal contents with saline preheated to 37°C, and then balance of 30 min with preheated Krebs–Ringer (K-R) solution and drug-containing test solution at the flow rate of 0.2 mL/min, respectively. Place a weighing EP tube containing the test solution at the entrance and another weighing EP tube at the exit to collect the perfusion fluid. The EP tube of the test solution and the EP tube of the collecting fluid were changed rapidly every 15 min, and the collection time was 0–120 min. Collect perfusion fluid and weigh it. At the end of the experiment, the corresponding intestinal segments were cut, and the intestinal segment length (l) and perimeter (r) were measured. The effects of low, middle and high concentrations (125, 250, 500 μg/mL) of paeonol solution and Pae-Lips, intestinal segments (duodenum, jejunum, ileum and colon) and different transporter inhibitors, including P-gp inhibitor verapamil (Ver, 100 μmol/L), MRP2 inhibitor indomethacin (Indo, 200 μmol/L) and BCRP inhibitor reserpine (Res, 50 μmol/L) on the absorption of paeonol and Pae-Lips were studied. The effective permeability coefficient (Papp) was calculated using the following formulas:

$$\text{Papp} = \frac{-\text{Q} \cdot \ln(\frac{\text{C}_{\text{out}}}{\text{C}_{\text{in}}} \cdot \frac{\text{V}_{\text{out}}}{\text{V}_{\text{in}}})}{2\pi\,\text{rl}}$$

$$\text{Ka} = (1 - \frac{\text{C}_{\text{out}}}{\text{C}_{\text{in}}} \cdot \frac{\text{V}_{\text{out}}}{\text{V}_{\text{in}}}) \cdot \frac{\text{Q}_{\text{in}}}{\pi \text{lr}^2}$$

where V_{in} and V_{out} are the volumes of the perfusate (mL) entering and leaving the intestine, respectively; Q_{in} is the perfusion flow rate; C_{in} and C_{out} are the drug concentrations in the perfused inlet and outlet, respectively; l and r are the length (cm) and radius (cm) of the perfused intestinal segment, respectively.

Caco-2 Cell Model

Cell Viability Using MTT Assay

MTT method was used to detect the cytotoxicity of paeonol and Pae-Lips to Caco-2 cells. Caco-2 cells were seeded in 96-well plates at a density of 10,000 cells per well, and the cells were incubated in a 5% CO_2 humidified incubator at 37°C. After 24 h incubation, the cells were, respectively, treated with increasing concentrations of paeonol and Pae-Lips, α-MEM was used as a negative control. After incubating for 4 hours, 10 μL of 0.5% MTT was added to each well and the plate was incubated at 37°C for 4 h, then discarded the supernatant, and 150 μL of DMSO was added to each well. The absorbance was measured at 490 nm. The percent of cell viability was measured from the equation as followed:

$$Cell\,viability(\%) = \frac{OD_{sample} - OD_{blank}}{OD_{control} - OD_{blank}} \times 100\%$$

Cell Culture in Transwell Chambers

Caco-2 cells were cultivated in α-MEM containing 20% fetal bovine serum, 1% non-essential amino acids, 4 mM-glutamine, 100 IU/mL penicillin and 100 μg/mL streptomycin at 37°C in an environment of 5% CO_2. After the cells were fused to 80%, the cells were inoculated in transwell chambers at a density of 10,0000 per well and cultivated for 21 days. The culture medium was changed every two days in the first week, and then every day thereafter. The TEER value was used to monitor the integrity of the single layer. Single layer TEER value higher than 300 $\Omega \cdot cm^2$ for experiment.

Transport Study in Caco-2 Cells

Transport studies were carried out in two directions, from the apical to the basolateral (AP to BL) and from the basolateral to the apical (BL to AP). After the monolayer was washed and balanced with preheated HBSS medium (pH 7.4), the different concentrations of paeonol solution (2.5, 5, 10 μg/mL) or Pae-Lips (2.5, 5, 10 μg/mL) were added to the apical side (AP, 0.5 mL) for the A to B direction or to the basolateral side (BL, 1.5 mL) for the B to A direction., and blank HBSS was added to the other side. After loading, the same amount of 0.2 mL samples were taken from the receiving side of BL or AP at different time points (30, 60, 90, 120, 150, 180 min). After each sampling, the same amount of HBSS was added to the receiving room to maintain a constant volume. In this study, we investigated the effects of different efflux inhibitors, P-gp inhibitor Ver (100 μmol/L), MRP2 inhibitor Indo (200 μmol/L) and BCRP inhibitor Res (50 μmol/L) on transport. All samples were kept at −80°C until analysis. The whole experiment was in triplicate.

The apparent permeability coefficient (Papp) and efflux ratio (ER) were determined using the following equation:

$$\text{Papp} = \frac{\Delta\text{Q}}{\Delta\text{t} \cdot \text{A} \cdot \text{C}_0}$$

$$\text{ER} = \frac{\text{Papp}_{(\text{BL}-\text{AP})}}{\text{Papp}_{(\text{AP}-\text{BL})}}$$

The value of ΔQ/Δt indicates the change in the cumulative amount of paeonol or Pae-Lips in the receiver solution. A represents the membrane surface area, and C_0 is refer to the initial drug.

Determination of Paeonol by LC-MS/MS

HPLC conditions: Shim-pack XR-ODSII column (75 mm × 3.0 mm, 5 μm), mobile phase is expressed by the ratio of methanol and water (v/v), which is 80:20, column temperature is set to 30°C. The flow rate is given by 0.8 mL/min, and the injection volume is 5 μL by using Shimadzu LC-20AD, which was attached to a Qtrap-4500 Mass Spectrometer (AB Sciex).

Mass spectrometry detection conditions: ESI as the source. In this procedure, negative ion detection is chosen as the detection method, multiple detection reaction monitoring (MRM). The optimized instrument parameters are as follows: the detection ion of paeonol had m/z 164.9–122.1, DP: −68 V, CE: −28 V, other MS parameters were: CUR: 30 psi, TEM: 550°C, GS1: 55 psi, GS2: 50 psi, CAD: medium.

Pae-Lips Inhibit Inflammation in RAW264.7 Macrophages Stimulated by LPS

Cell Culture of RAW 264.7

RAW264.7 cells are in DMEM containing 20% fetal bovine serum, 1% non-essential amino acids, 4 mM L-glutamine, 100 IU/mL penicillin and 100 μg/mL streptomycin. Incubate at 37°C in a constant temperature incubator with 5% CO_2. The cells were passaged by trypsinization until the cells were 90% confluent.

Cell Viability Assay

Take log phase RAW 264.7 macrophages and inoculate them in 96-well plates at a cell density of 10,000 cells per well. After culturing for 24 hours in an incubator, aspirate the supernatant and administer 100 μL per well (different concentrations of paeonol or Pae-Lips), each group was set with 6 repetitive holes. After acting for 24 hours the supernatant was aspirated, 10 μL 0.5% MTT was added to each well, another 4 hours was needed for incubating, and then discarded the supernatant, and added 150 μL dimethyl sulfoxide to each well. The absorbance was measured at 490 nm.

NO Release and Enzyme Immunoassay of TNF-a, IL-6 and IL-10

RAW264.7 cells were seeded in 96-well plates at a density of 15,000 cells per well. After 24 hours of incubation, the supernatant was discarded. Divided into control group, LPS group and administration group, the administration group is paeonol group (final concentration was 5 μg/mL), low concentration of Pae-Lips group (Pae-Lips-L, final concentration was 2.5 μg/mL), middle concentration of Pae-Lips group (Pae-Lips-M, final concentration was 5 μg/mL), high concentration of Pae-Lips group (Pae-Lips-H, final concentration was 10 μg/mL). After 2 hours of incubation, all groups except the control group were incubated with LPS (final concentration was 1 μg/mL). After 20 hours, the supernatant was collected to detect the NO content according to the NO kit, and the ELISA kit was used to detect mouse interleukin 6 (IL-6), tumor necrosis factor α (TNF-α) and interleukin 10 (IL-10) content.

Anti-Inflammatory Effect of Pae-Lips on UC Induced by DSS

DSS Model of Mouse Colitis

Forty-two male Balb/c mice (10 weeks old) were adaptively reared for 1 week and randomly divided into 7 groups (n = 6): normal control group, DSS model group, SASP group (500 mg/kg), paeonol group (200 mg/kg), Pae-Lips-L (100 mg/kg), Pae-Lips-M (200 mg/kg), Pae-Lips-H (400 mg/kg). The drug is administered by gavage, once in the morning and once in the evening, suspended in 0.5% CMC-Na. Except for the normal control group who drank tap water freely, all the other groups drank 3% (w/v) DSS. The entire treatment program lasts for 7 days.

Enzyme Immunoassay Assay of TNF-a, IL-6 and IL-10

On the 8th day, the eyes of the mice were removed and blood was collected, and the separated serum was stored at −80°C. The Elisa kit detects serum levels of IL-6, TNF-α, and IL-10.

Disease Activity Index (DAI) and Colon Length

DAI is used to assess the symptoms of mice based on daily weight loss, stool consistency, and bleeding. The entire colon was separated and measured for length, then cut longitudinally and fixed in 10% formaldehyde.

Histological Examination

The distal colon was separated about 2 cm in length for histological examination. All sections were fixed with 10% formaldehyde and then stained with hematoxylin-eosin (HE). Comprehensive analysis of pathological changes according to the severity of intestinal wall inflammation, the extent of lesions and the degree of crypt.

Immunohistochemistry (IHC)

Colon tissue sections were used for IHC analysis. Briefly, NF-κB (1:100) and p38 MAPK (1:150) were used to detect protein expression in colon tissue, DAB staining showed positive expression reflected as brownish yellow, and the slides were counterstained with hematoxylin. Protein levels were calculated using Image-Pro Plus 6.0 software to calculate the integrated optical density (IOD) value at five (200×) fields.

Results

Preparation and Optimization of Pae-Lips

The test was designed by the Box-Behnken response surface method of the Design Expert 12 analysis software. The level arrangement of each factor is shown in Table S1. The test arrangement and results are shown in Table S2. EE% is the response value for model fitting, and the fitting equation is obtained as EE% = 89.77–0.4587A - 0.9112B - 0.4850C - 1.13AB + 1.08AC + 0.3657BC - $3.01A^2$ - $4.37B^2$ - $1.78C^2$ (r^2 = 0.9939, $p < 0.001$), analysis of variance was performed on the model, and the results are shown in Table S3. It can be seen from the table that the model is significant ($p < 0.05$), and the lack of fit test of the model is not significant ($p > 0.05$), indicating that the model fits well and can better predict the best prescription. According to the software prediction of the best process, combined with the actual conditions, the verification test was carried out. Repeat three times to determine the best process: SPC: CHOL (6:1); paeonol concentration 3 mg/mL, the pH of PBS value is 6.5.

According to the equation fitting results, the 3D effect surface map and contour map of the response surface are obtained, and the results are shown in Figure S1. Both the 3D effect surface map and the contour map are curved to different degrees, indicating that the interaction of the three factors affects the sealing rate.

Characterization of the Pae-Lips

The preparation of Pae-Lips was shown above, the EE% measured by ultrafiltration centrifugation method was 90.20% ± 0.37%; the DL% was 9.62% ± 0.44%; the particle size measured by the laser particle size analyzer was 171.9 ± 8.7 nm (Figure 1A), the Zeta potential was −10.9 mV (Figure 1B) and the PDI of 0.223 ± 0.024 and low values confirmed its narrow particle size distribution.

The TEM image (Figure 1C) showed that Pae-Lips were spherical with uniform size distribution and the particle size further verified the value measured by the particle size analyzer.

In the DSC thermogram (Figure 1D) of Pae-Lips, the endothermic peak (190°C) of paeonol disappeared, indicating that paeonol was entrapped inside the bilayer in liposomes; in the XRD pattern of Pae-Lips (Figure 1E), the diffraction peak (10°) of paeonol disappeared, further indicating that paeonol has been encapsulated in the phospholipid bilayer to form liposomes. The peak of paeonol at 1633 cm^{-1} was the aryl ketone carbonyl stretching vibration peak (C=0). In the Pae-Lips diagram, the peak intensity of this peak was significantly reduced or even disappeared (Figure 1F), indicating that Lips had a shielding effect on paeonol. Paeonol has been successfully loaded into Liposomes.

The results of the in vitro release test are shown in Figure 2A. Compared with the paeonol suspension, the cumulative release percentage (P%) of the drug-loaded liposomes in PBS (pH 7.4) for 24 hours increased from

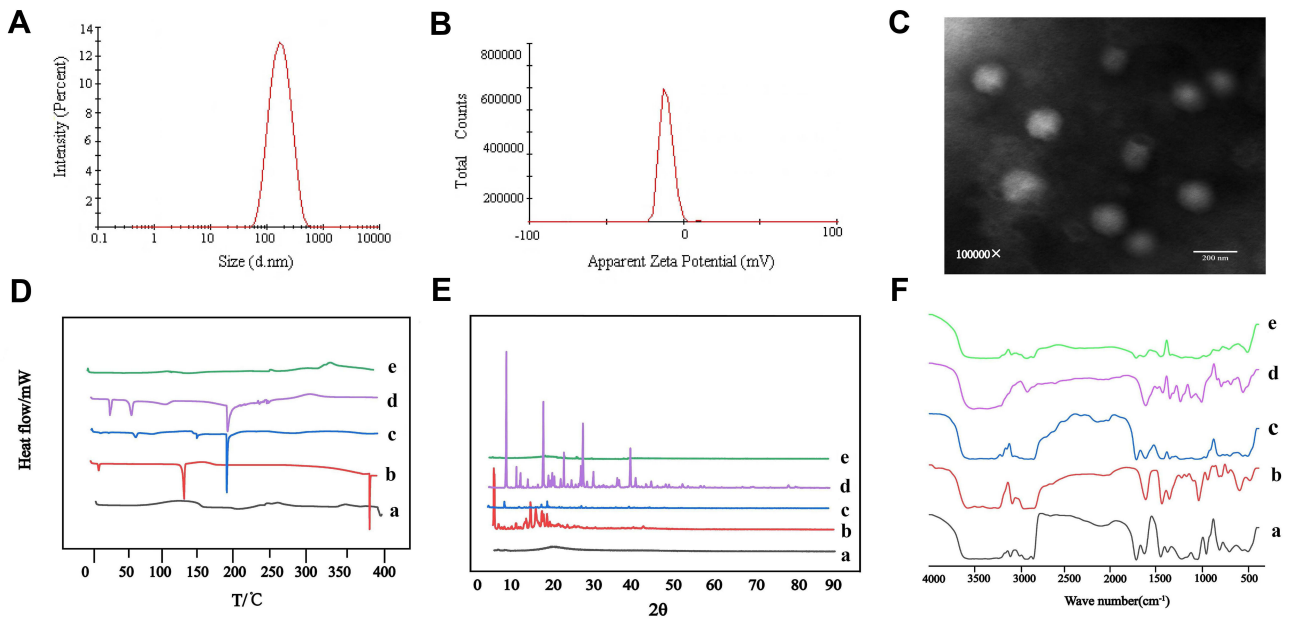

Figure 1 Characterization of the Pae-Lips. (**A**) The particle size distribution of Pae-Lips. (**B**) The zeta potential of Pae-Lips. (**C**) TEM images of Pae-Lips. (**D**) DSC. (**E**) XRD. (**F**) FTIR.
Notes: (a) SPC, (b) CHOL, (c) PM, (d) paeonol, (e) Pae-Lips.

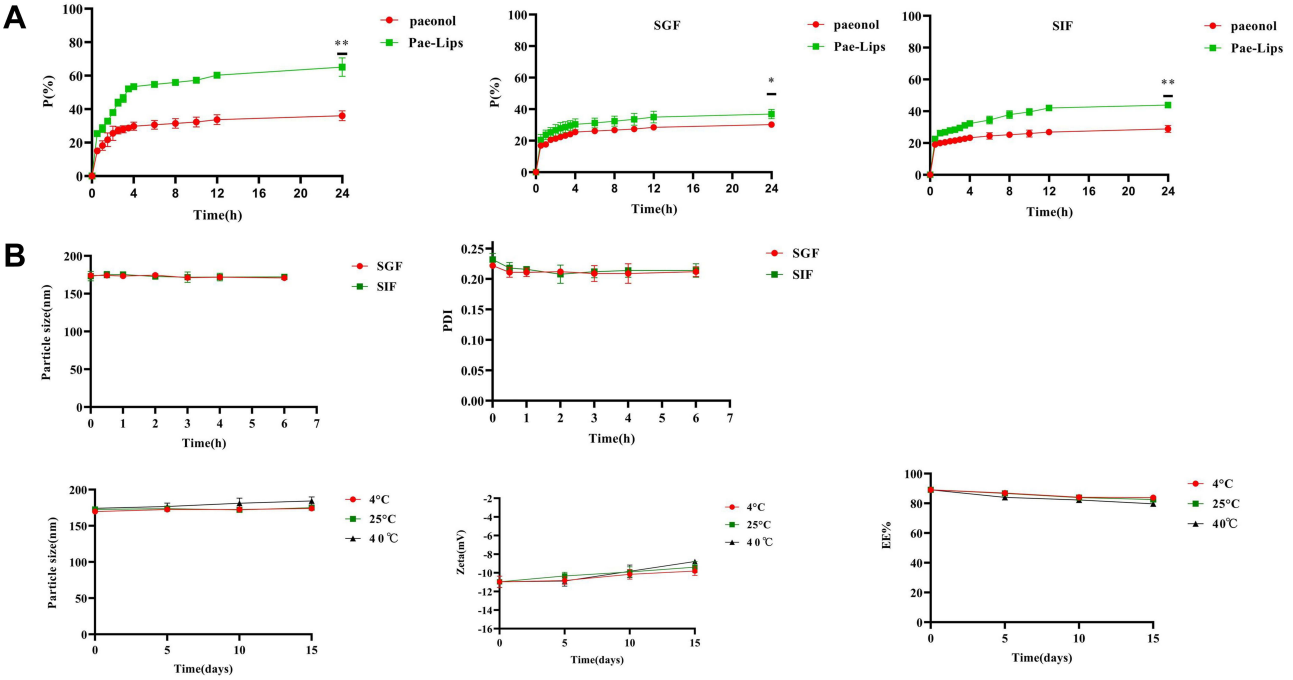

Figure 2 (**A**) In vitro release curve of paeonol and Pae-Lips. (**B**) The stability of Pae-Lips at SGF, SIF and different temperatures.
Notes: The data were presented as the mean ± SD (n = 3). Compared with the paeonol group, *$p < 0.05$, **$p < 0.01$.

(36.05 ± 2.94) % to (65.11 ± 5.5) %, SGF and SIF also increased significantly, indicating that liposomes can improve the dissolution of paeonol, and Table 1 shows that release mechanism of paeonol and drug-loaded liposomes conformed to the first-order kinetic model, that is, passive diffusion. The stability test results are shown in Figure 2B. Pae-lips are basically stable within 15 days, and the stability is the best at 4°C, which may

Table 1 Cumulative Release Percentage-Time Model Fitting Equation

Sample	Fitting model	Fitting equation	*r*
Paeonol	Zero-order kinetic model	$p = 0.7137t + 23.281$	0.5731
	First-order kinetic model	$Ln(1\text{-}p) = -0.1644t - 0.8096$	0.8957
	Higuchi model	$p = 0.1278t^{1/2} + 0.4861$	0.7714
	Hixcon-Crowell model	$(100\text{-}p)^{1/3} = -0.0138t + 4.2481$	0.5986
Pae-Lips	Zero-order kinetic model	$p = 1.519t + 38.089$	0.6024
	First-order kinetic model	$Ln(1\text{-}p) = -0.1705t - 0.6373$	0.8874
	Higuchi model	$p = 0.1494t^{1/2} + 0.3994$	0.7979
	Hixcon-Crowell model	$(100\text{-}p)^{1/3} = -0.0372t + 3.9529$	0.6621

be related to the low system energy and low phospholipid oxidation rate under low temperature environment. Therefore, Pae-lips were stored at 4°C.

In vivo Pharmacokinetic Studies

The plasma concentration-time curves of paeonol suspension and Pae-Lips are shown in Figure 3, and the pharmacokinetic parameters are shown in Table 2. The $AUC_{(0\text{-}t)}$ of Pae-Lips is significantly higher than paeonol, which was increased by 2.78 times. Compared with paeonol, the C_{max} of Pae-Lips was increased by 2.56 times, and $t_{1/2}$ was extended from 3.37 h to 10.69 h. These results confirmed that the oral absorption of Pae-Lips was better than that of paeonol suspension. Pae-Lips can improve the oral bioavailability of paeonol and has a sustained release effect.

In situ SPIP Study

SPIP was used to study the intestinal absorption of paeonol suspension and Pae-Lips. As shown in the Figure 4A and Table 3, the Papp and Ka values of Pae-Lips in the duodenum, jejunum, ileum and colon were all higher than that of paeonol suspension at different dosages. Pae-Lips significantly increased the Papp of colonic at low, medium and high doses, and the Papp of ileum increased significantly at low and medium doses. These showed that Pae-Lips can improve the intestinal absorption of paeonol.

There was no significant difference in the Papp values of paeonol suspension at different concentrations, which indicated that the absorption mechanism of paeonol was mainly passive diffusion. As shown in the Figure 4B–D, after adding Ver, Indo and Res, the Papp of paeonol suspension in each intestinal segment was significantly increased, indicating that paeonol may be a substrate of P-gp, MRP2 and BCRP. However, the Papp value of Pae-Lips did not change significantly, which may be due to the special structure of liposomes.

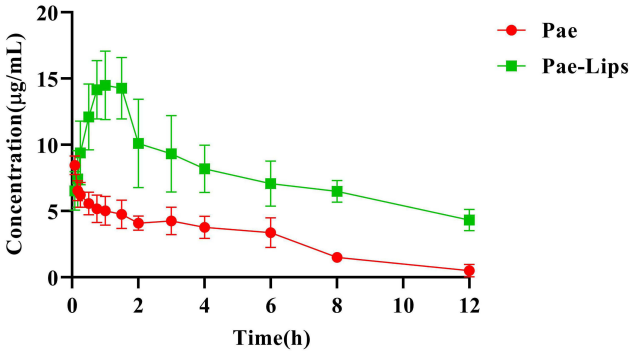

Figure 3 Paeonol and Pae-Lips plasma concentration-time curves.
Note: The data were presented as the mean ± SD (n = 6).

Table 2 Pharmacokinetic Parameters of Paeonol and Pae-Lips

Parameters	Unit	Paeonol	Pae-Lips
$t_{1/2}$	h	3.37 ± 1.20	10.69 ± 5.58*
C_{max}	μg/mL	8.46 ± 0.70	21.67 ± 1.26***
$AUC_{(0-t)}$	μg/mL·h	33.60 ± 7.56	93.33 ± 14.99***
$AUC_{(0-\infty)}$	μg/mL·h	38.59 ± 6.71	162.22 ± 38.11***
$MRT_{(0-t)}$	h	3.83 ± 0.61	4.92 ± 0.28**
CLz/F	L/h/kg	2.65 ± 0.41	0.64 ± 0.14***

Notes: the data were presented as the mean ± SD (n = 6). Compared with the paeonol suspension, *$p < 0.05$, **$p < 0.01$, ***$p < 0.001$.

Caco-2 Cell Model

Cytotoxicity Test Results

MTT method was used to detect the influence of paeonol and Pae-Lips on cell viability. The survival rate of cells within 10 μg/mL was greater than 90%. When the administration concentration exceeds 10 μg/mL, the cell viability was significantly reduced (Figure 5). Therefore, transportation studies were conducted at concentrations of 2.5, 5, 10 μg/mL.

Transport Test Results

The Caco-2 monolayer cell model was used to study drug delivery. The paeonol solution and Pae-Lips were transported in two directions. The effect of different concentrations on the Papp values of paeonol and Pae-Lips are shown in Figure 6A. The effect of efflux transporter inhibitors on the Papp values of paeonol and Pae-Lips are shown in Figure 6B-D. The transport volume of paeonol and Pae-Lips in the direction of AP-BL at 2.5 μg/mL, 5 μg/mL and 10 μg/mL are shown in Figure 7. The Papp value (AP-BL) of paeonol at low, medium and high concentrations were (3.25 ± 0.32, 3.62 ± 0.13, 3.65 ± 0.52) × 10^{-6} cm/s, the Papp value (AP-BL) of Pae-Lips was (4.59 ± 0.20, 4.42 ± 0.35, 5.57 ± 0.90) × 10^{-6} cm/s, which were an increase of 1.47, 1.22 and 1.53 times,

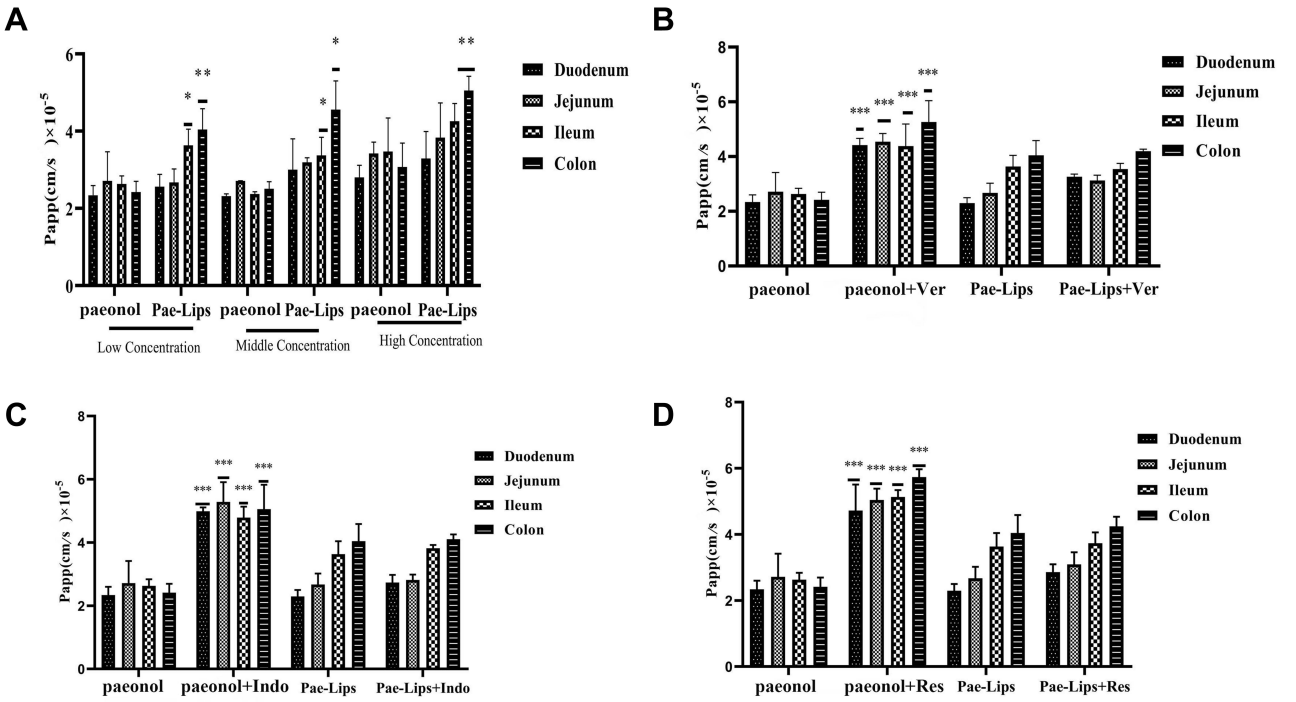

Figure 4 The effect of concentrations and efflux transporter inhibitors on the Papp values of Paeonol and Pae-Lips. (**A**) Low, medium and high concentration. (**B**) Added P-gp inhibitor, verapamil (Ver). (**C**) Added MRP2 inhibitor, indomethacin (Indo). (**D**) Added BCRP inhibitor, reserpine (Res).
Notes: The data were presented as the mean ± SD (n = 3). Compared with the paeonol group, *$p < 0.05$, **$p < 0.01$, ***$p < 0.001$.

Table 3 Ka Values of Different Concentrations of Paeonol and Pae-Lips

Concentration (μg/mL)	Group	Duodenum ($\times 10^{-4}$ cm/s)	Jejunum ($\times 10^{-4}$ cm/s)	Ileum ($\times 10^{-4}$ cm/s)	Colon ($\times 10^{-4}$ cm/s)
125	Pae	1.58 ± 0.16	1.80 ± 0.26	1.84 ± 0.06	1.69 ± 0.33
	Pae-Lips	1.62 ± 0.23	1.81 ± 0.08	2.50 ± 0.05***	2.54 ± 0.17***
250	Pae	1.36 ± 0.10	1.63 ± 0.004	1.47 ± 0.03	1.57 ± 0.04
	Pae-Lips	1.75 ± 0.23	1.97 ± 0.11	2.19 ± 0.31*	2.74 ± 0.18***
500	Pae	1.39 ± 0.05	1.75 ± 0.03	1.86 ± 0.20	1.80 ± 0.29
	Pae-Lips	1.47 ± 0.10	1.81 ± 0.21	2.02 ± 0.15	2.26 ± 0.22

Notes: the data were presented as the mean ± SD (n = 3). Compared with the paeonol group, *$p < 0.05$, ***$p < 0.001$.

significantly improved the penetration efficiency of paeonol and promoted absorption ($p < 0.05$). Moreover, the transport volume of paeonol and Pae-Lips (AP-BL) gradually accumulates with concentration and time, and the transport volume of Pae-Lips was higher than that of paeonol, indicating that Pae-Lips had better transport capacity.

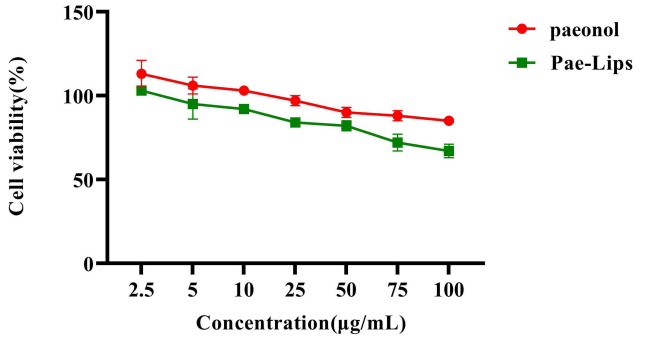

Figure 5 Effects of paeonol and Pae-Lips on the cell viability of Caco-2 cells.

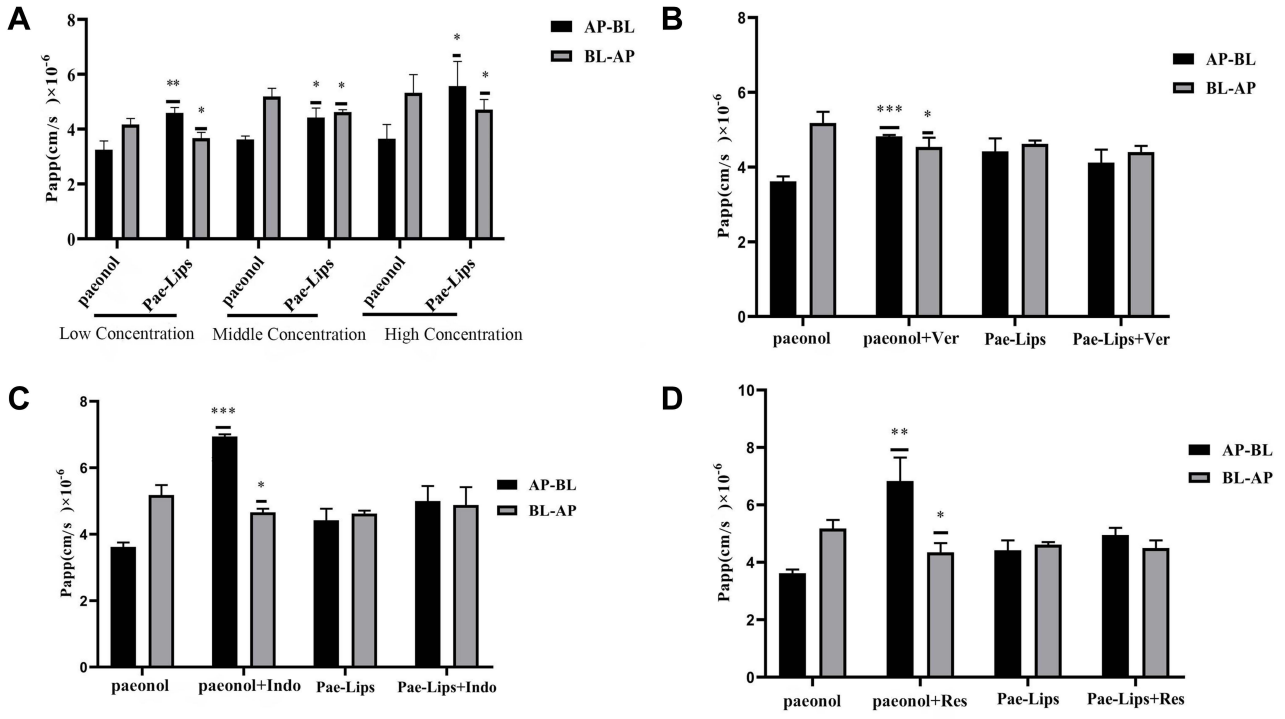

Figure 6 The effect of concentrations and efflux transporter inhibitors on the Papp values of paeonol and Pae-Lips. (**A**) Low, medium and high concentration. (**B**) P-gp inhibitor. (**C**) MRP2 inhibitor. (**D**) BCRP inhibitor.
Notes: The data were presented as the mean ± SD (n = 3). Compared with the paeonol group, *$p < 0.05$, **$p < 0.01$, ***$p < 0.001$.

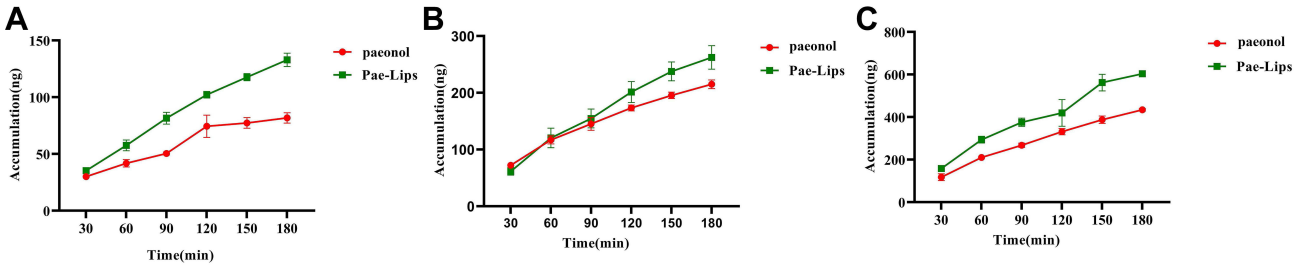

Figure 7 Transport volume of paeonol and Pae-Lips in the direction of AP-BL at 2.5 μg/mL (**A**), 5 μg/mL (**B**) and 10 μg/mL (**C**).

In addition, the Papp value (BL-AP) of paeonol at low, medium, and high concentrations were (4.17 ± 0.22, 5.19 ± 0.30, 5.32 ± 0.67) × 10^{-6}cm/s, and the Papp value of Pae-Lips (BL-AP) was (3.67 ± 0.21, 4.62 ± 0.09, 4.71 ± 0.37) ×10^{-6}cm/s, respectively. The ER values of Paeonol and Pae-Lips were both less than 1.5. Generally speaking, we believe that ER >1.5 may involve active transportation. Therefore, the transportation mechanism may be passive diffusion, involving efflux transportation.

When different inhibitors and drugs were used together, Ver, Indo, and Res significantly increased Papp value of paeonol (AP-BL) on average; while Papp value of Pae-Lips (AP-BL) had no significant effect. These results indicated that paeonol may be a substrate of P-gp, MRP2 and BCRP. However, Pae-Lips, due to the phospholipid bilayer structure, avoided the efflux of efflux proteins, thereby enhancing absorption.

Anti-Inflammatory Ability of Pae-Lips on LPS-Induced RAW264.7 Cells

Cell Viability Research

As shown in Figure 8. the cytotoxicity was measured by the MTT method, and the cell viability >80% was selected for the experiment. The concentration of paeonol solution was 5 μg/mL, and the concentration of Pae-Lips was 2.5, 5, 10 μg/mL.

NO Release and Enzyme Immunoassay of TNF-a, IL-6 and IL-10

As shown in Figure 9, LPS stimulated RAW264.7 macrophages significantly increased the levels of NO and pro-inflammatory factors IL-6 and TNF-α, while after adding paeonol solution and Pae-Lips treatment, the concentration-dependent decreased ($p < 0.05$). The NO content and inflammatory factor levels of Pae-Lips-M and Pae-Lips-H were significantly lower than the paeonol solution group ($p < 0.05$). While the level of anti-inflammatory factor IL-10 increased in a concentration-dependent manner, Pae-Lips-M and Pae-Lips-H were significantly higher than paeonol solution ($p < 0.05$).

The above results showed that both paeonol solution and Pae-Lips have obvious anti-inflammatory effects, and the anti-inflammatory effect was stronger with the increase of drug concentration, the anti-inflammatory effect of Pae-Lips was significantly better than that of paeonol solution.

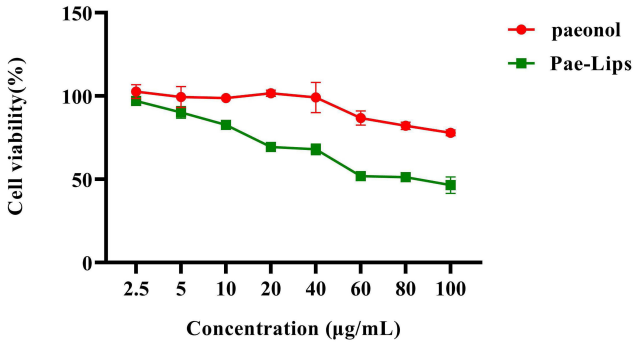

Figure 8 Effects of paeonol and Pae-Lips on the cell viability of RAW264.7 cells.

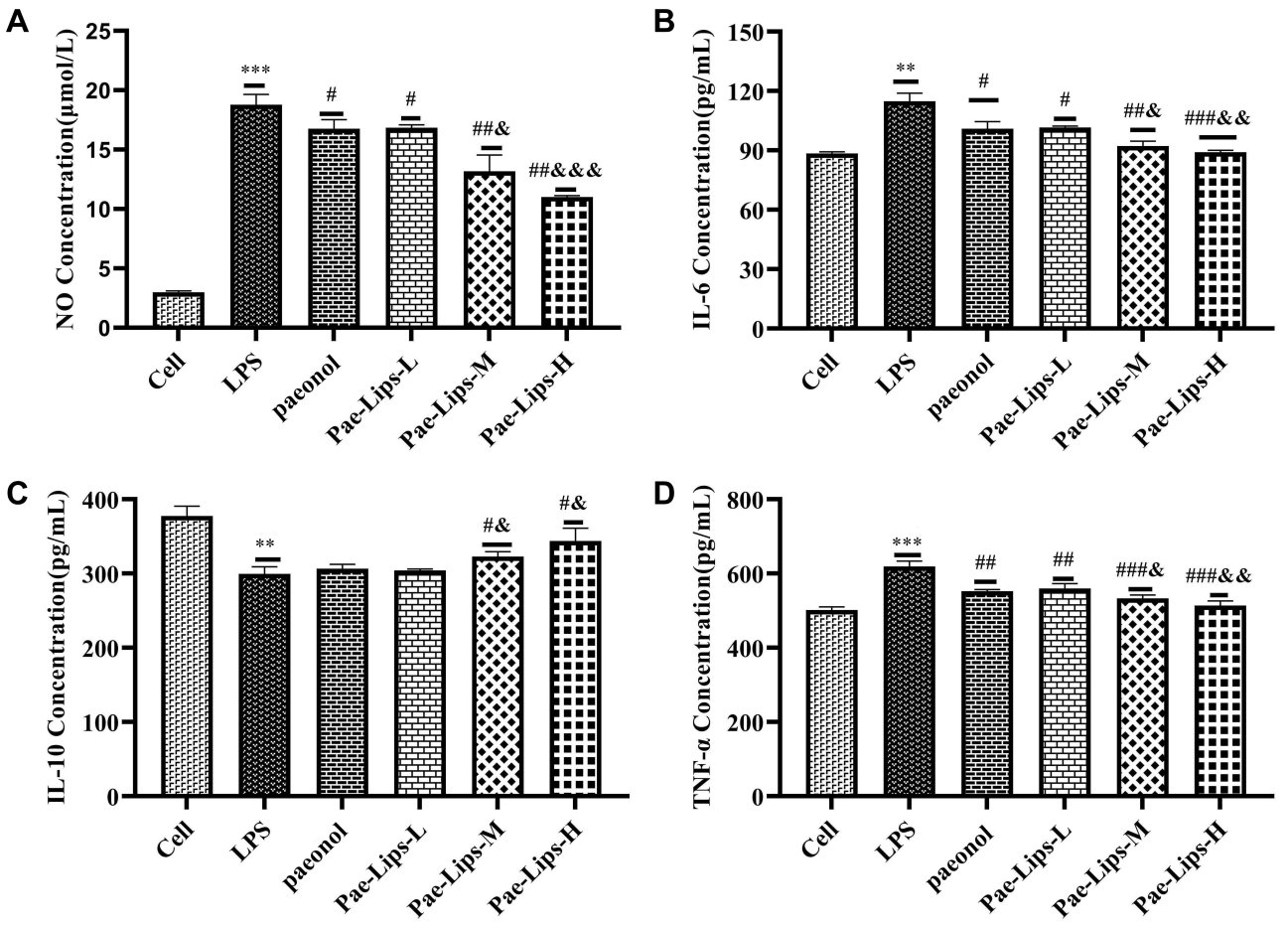

Figure 9 The levels of NO (**A**), IL-6 (**B**), IL-10 (**C**), TNF-α (**D**) in RAW264.7 cells.

Notes: The data were presented as the mean ± SD (n = 3). Compared with the Cell group, $^{**}p < 0.01$, $^{***}p < 0.001$; compared with the LPS group, $^{\#}p < 0.05$, $^{\#\#}p < 0.01$, $^{\#\#\#}p < 0.001$; compared with the paeonol group, $^{\&}p < 0.05$, $^{\&\&}p < 0.01$, $^{\&\&\&}p < 0.001$.

Anti-Inflammatory Effect of Pae-Lips on UC Induced by DSS

DAI and Colon Length

The DAI was used to evaluate the symptoms of mice. As shown in Table 4, compared with the Model group, the DAI of the drug treatment group was reduced, and all reached statistical significance on the 7th day ($p < 0.05$). Generally, the length of the colon will shrink due to inflammatory infiltration, which will be improved after drug treatment. Figure 10 shows that the colon length of the Model group and Pae-Lips-L group was significantly shorter than that of the Control group ($p < 0.01$), while the colon length of the other treatment groups was significantly higher than that of the Model group ($p < 0.05$), and there was no significant difference from the Control group.

Table 4 The Disease Activity Index (DAI) Score

Days	Control	Model	SASP	Paeonol	Pae-Lips-L	Pae-Lips-M	Pae-Lips-H
1	0	0.83 ± 0.27	0.61 ± 0.26	0.75 ± 0.27	0.67 ± 0.26	0.58 ± 0.20	0.67 ± 0.26
2	0	1.58 ± 0.58	1.06 ± 0.41	1.50 ± 0.45	1.25 ± 0.69	1.17 ± 0.41	1.08 ± 0.49
3	0	2.83 ± 0.93	1.18 ± 0.26	2.58 ± 0.80	1.67 ± 0.87	1.50 ± 0.55	1.50 ± 0.55
4	0	3.92 ± 0.66	2.46 ± 0.69	3.25 ± 0.76	2.58 ± 0.86	2.75 ± 0.76	2.67 ± 0.61
5	0	5.33 ± 0.82	3.42 ± 0.80	4.92 ± 0.59	5.50 ± 0.84	3.92 ± 0.59	3.75 ± 0.52
6	0	7.33 ± 0.61	3.22 ± 0.52	5.83 ± 0.68	6.42 ± 0.80	4.42 ± 0.58	3.75 ± 0.61
7	0	8.75 ± 0.82	3.48 ± 0.86$^{\#\#\#}$	5.75 ± 0.82$^{\#\#}$	6.92 ± 0.66$^{\#}$	4.92 ± 0.49$^{\#\#\&}$	4.08 ± 0.86$^{\#\#\#\&\&}$

Notes: The data were presented as the mean ± SD (n = 6). Compared with the Model group, $^{\#}p < 0.05$, $^{\#\#}p < 0.01$, $^{\#\#\#}p < 0.001$; compared with the paeonol group, $^{\&}p < 0.05$, $^{\&\&}p < 0.01$.

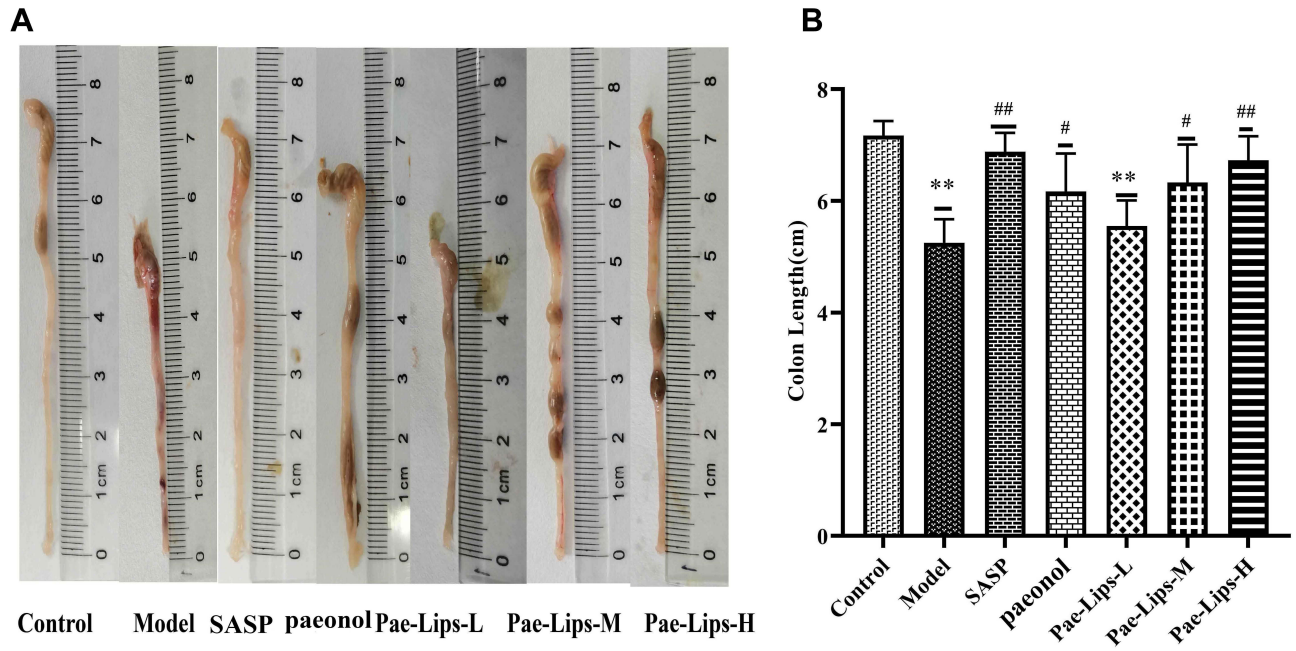

Figure 10 Colon length measurement.(**A**) Representative photos of colon lengths for different groups. (**B**) Quantitative analysis of colon length in different groups.
Notes: The data were presented as the mean ± SD (n = 6). Compared with the Control group, $^{**}p < 0.01$; Compared with the Model group, $^{\#}p < 0.05$, $^{\#\#}p < 0.01$.

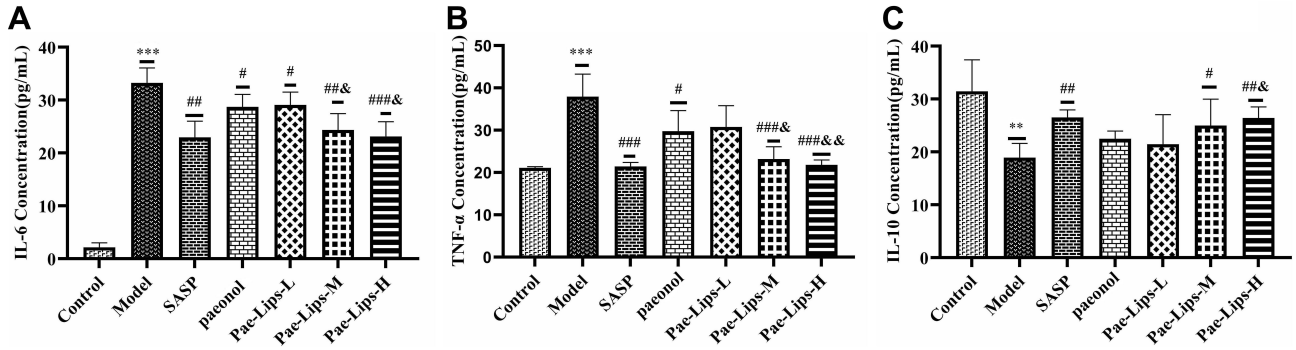

Figure 11 The levels of IL-6 (**A**), TNF-α (**B**) and IL-10 (**C**) in the serum of Balb/c mice.
Notes: The data were presented as the mean ± SD (n = 6). Compared with the Control group, $^{**}p < 0.01$, $^{***}p < 0.001$; compared with the Model group, $^{\#}p < 0.05$, $^{\#\#}p < 0.01$, $^{\#\#\#}p < 0.001$; compared with the paeonol group, $^{\&}p < 0.05$, $^{\&\&}p < 0.01$.

Enzyme Immunoassay of TNF-a, IL-6 and IL-10

As shown in Figure 11, compared with the Control group, the levels of IL-6 and TNF-α in the Model group were significantly increased, and the level of IL-10 was significantly decreased, indicating that the DSS-induced mouse UC model was successfully constructed. After drug treatment, compared with the Model group, the levels of IL-6 and TNF-α in each drug treatment group were decreased, and the level of IL-10 was increased. The Pae-Lips group showed a concentration-dependent change with the increasing dose. Compared with the paeonol suspension, the levels of IL-6 and TNF-α in Pae-Lips-M and Pae-Lips-H were significantly decreased, the IL-10 level in Pae-Lips-H group was significantly increased.

Histological Examination

Histopathology was analyzed to assess the damage to the colonic mucosa, including severity of bowel wall inflammation, extent of lesion involvement, and degree of crypt damage. In normal mice, the wall mucosa epithelial cells were intact, without ulcers, the lamina propria had no inflammatory cell infiltration, and no obvious lesions were found in other layers. After DSS induction, inflammatory cells in the colon of mice in the model group infiltrated and invaded the

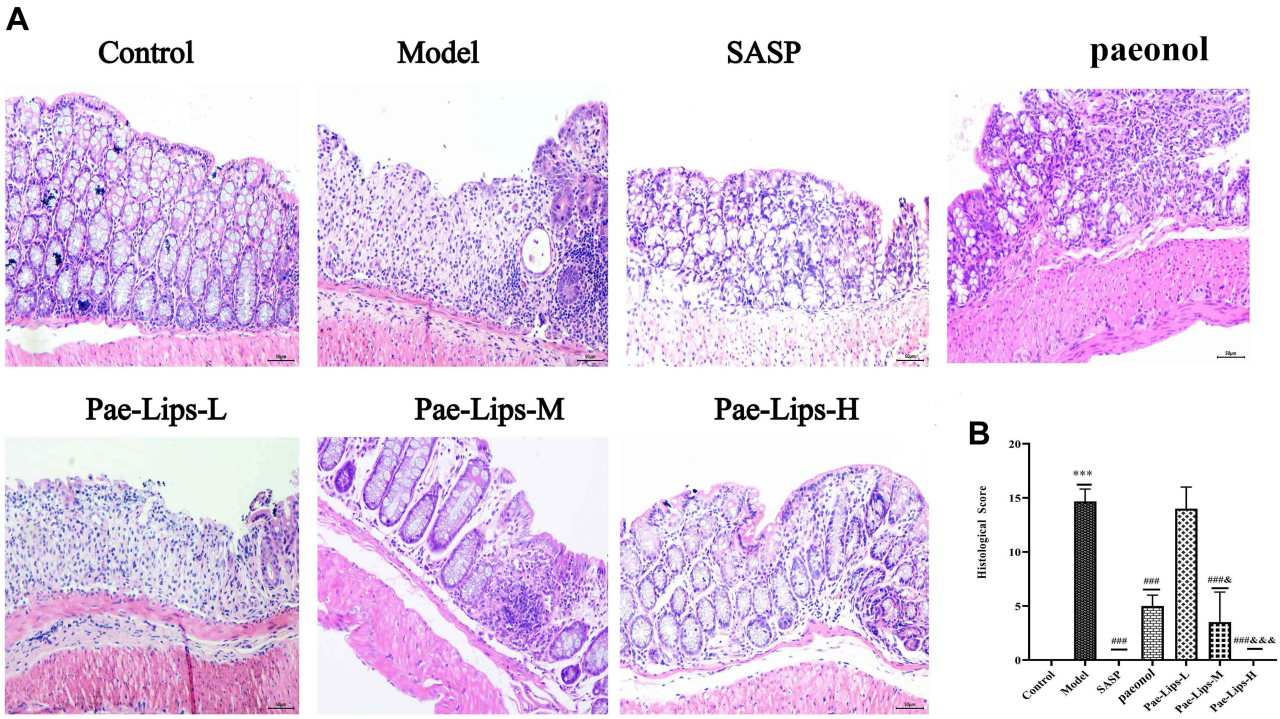

Figure 12 (**A**) Colon tissue H&E staining, and representative pictures. Scale bars, 50 μm, (200 ×). (**B**) Histopathological scores were calculated.
Notes: The data were presented as the mean ± SD (n = 3). Compared with the Control group, $^{***}p < 0.001$; compared with the Model group, $^{\#\#\#\#}p < 0.001$; compared with the paeonol group, $^{\&}p < 0.05$, $^{\&\&\&}p < 0.001$.

submucosa and the crypts were severely damaged. The administration groups showed mild colon damage and lower histological scores, and no obvious lesions were found in the SASP group and Pae-Lips-H group. Compared with the paeonol group, the colonic lesions in the Pae-Lips-M and Pae-Lips-H groups were significantly improved (Figure 12).

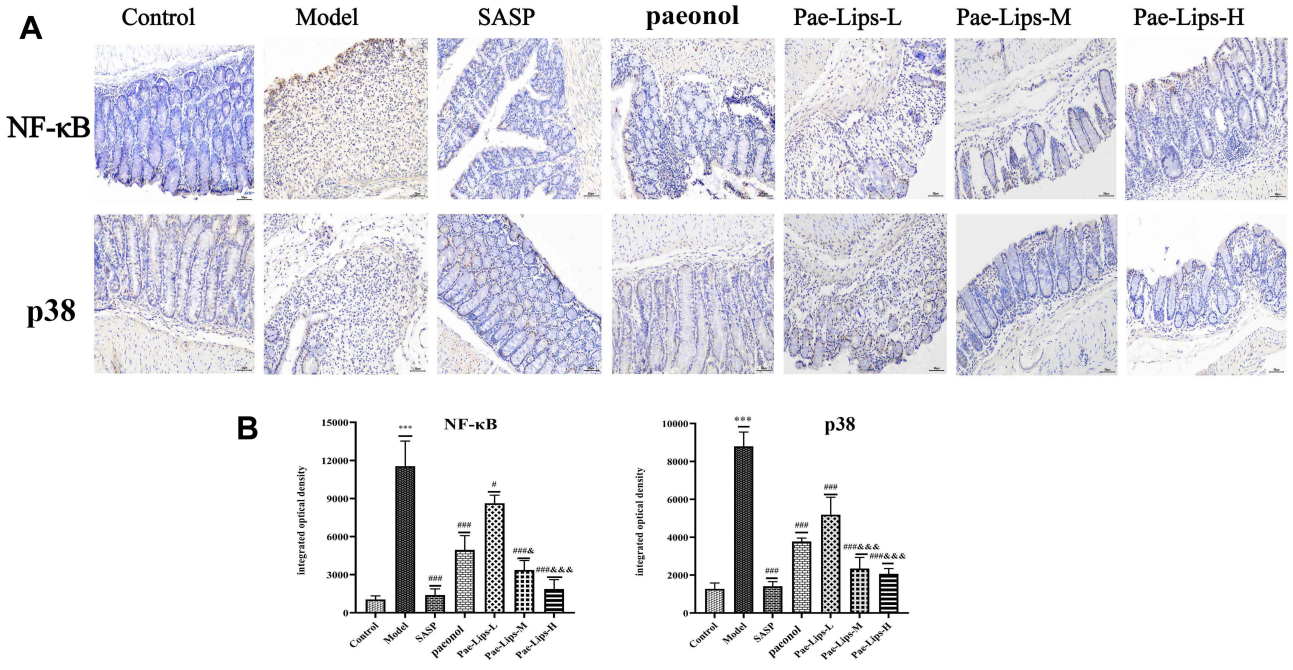

Figure 13 (**A**) Representative images of IHC staining of NF-κB and p38 proteins in colon tissue. Scale bar, 50 μm (200 ×); (**B**) IOD values.
Notes: The data were presented as the mean ± SD (n = 5). Compared with the Control group, $^{***}p < 0.001$; compared with the Model group, $^{\#}p < 0.05$, $^{\#\#\#\#}p < 0.001$; compared with the paeonol group, $^{\&}p < 0.05$, $^{\&\&\&}p < 0.001$.

Immunohistochemistry

As shown in Figure 13, compared with the Control group, the expression of NF-κB and p38 in the Model group was significantly up-regulated ($p < 0.001$). After drug treatment, this up-regulation was significantly inhibited ($p < 0.05$), and compared with the paeonol group, Pae-Lips-M and Pae-Lips-H groups were significantly down-regulated ($p < 0.05$). The cytokine levels regulated by paeonol and Pae-Lips were closely related to the expression of NF-κB and p38. Previous studies have suggested that the potential anti-colitis mechanism of paeonol may involve inhibition and transactivation of NF-κB/STAT1[26] and MAPK/ERK/p38 pathways.[17] Our findings are consistent with those reported in the literature.

Discussion

Now, there are paeonol tablets, paeonol ointments, paeonol patches and paeonol injections on the market. However, paeonol has poor water solubility and fast metabolism, resulting in low bioavailability.[30] Compared with injections, paeonol tablets, ointments and patches have low bioavailability, but injections contain high concentrations of tween 80 and ethanol to stimulate blood vessels and muscles.[31] Modern research has used nanotechnology,[32,33] cyclodextrin inclusion,[20] and derivatization technology to modify it.[34] Although these preparation techniques have improved the problem of low bioavailability of paeonol, there is a lack of relevant pharmacodynamic experiments to verify the anti-inflammatory effects of their preparations. The most remarkable advantages of liposomes are their biocompatibility and safety due to resemblance to biomembranes. Moreover, the oral absorption of the drug can be improved. Therefore, after making paeonol into Pae-Lips, we not only studied the changes of its absorption, but also studied its anti-inflammatory activity in vivo and in vitro. First, optimized liposome preparation process through Box-Behnken effect surface method, the morphology of Pae-Lips was characterized by TEM, and the liposome structure of Pae-Lips was characterized by DSC, XRD and FTIR. The results showed that paeonol had successfully entered the phospholipid bilayer to form Pae-Lips. The results of in vitro stability experiments and in vitro drug release experiments showed that liposomes have good stability in SGF and SIF, and the drug dissolution of Pae-Lips is significantly enhanced. In vivo pharmacokinetic experiments found that Pae-Lips significantly increased the AUC, C_{max} and $t_{1/2}$ of paeonol, which proved that liposome formulations can prolong the action time of the drug, increase absorption, and improve oral bioavailability. Then, through the Caco-2 monolayer cell model and SPIP experiment, the absorption mechanism of paeonol was further explored from the cell level and the intestinal level. The results of the study found that the preparation of paeonol liposomes significantly improved the intestinal absorption of paeonol. It showed that when the drug with poor water solubility was administered, it could be made into liposome to improve its oral absorption.[35] Caco-2 cells are derived from human colon cancer and can form monolayers in vitro and differentiate into the luminal side (AP) and the basolateral side (BL). The differentiated cells are similar in shape and function to the human small intestine, have good homology, and the Caco-2 cell culture method is simple, time-saving and economical, and has been widely used in the screening of new drugs and the study of drug absorption mechanisms.[36] In this paper, the transport of paeonol and Pae-Lips at different concentrations and the addition of inhibitors were discussed from in vitro cell-level studies through the Caco-2 monolayer cell model. The results showed that the Papp value (AP-BL) of Pae-Lips was significantly increased, and the absorption of paeonol was significantly improved. After adding the inhibitor, the absorption of paeonol was significantly improved, but there was no significant change in Pae-Lips, which might be the structure of the Lips prevented paeonol from being recognized for efflux. The absorption mechanism of paeonol is passive diffusion and involves efflux transport.

The intestine, as the main absorption site for oral administration, is an important prerequisite for oral efficacy. In addition to the physical and chemical properties of the drug itself, the barrier function of intestinal epithelial cells also directly affects the bioavailability of oral drugs, and the barrier function of the intestine depends on the specific membrane transport protein.[37,38] P-glycoprotein (P-gp), multidrug resistance protein 2 (MRP2) and breast cancer resistance protein (BCRP) are the main ABC transporters distributed in the intestinal barrier.[39,40] Among them, P-gp is most expressed in the colon and ileum, and MRP2 and BCRP are highly expressed in the small intestine.[41] The drug efflux mediated by these ABC transporters limits the absorption of the substrate drug and has a significant impact on the efficacy of oral drugs. Therefore, it is necessary to clarify the relationship between the effective ingredients of traditional Chinese medicine and these proteins, and on this basis, add related inhibitors[41,42] or modify their structure to improve the absorption in the gastrointestinal tract.[43,44] In situ SPIP represents the natural

environment of the intestine to a certain extent and provides the closest situation to oral administration.[45] The results showed that after making paeonol into Pae-Lips or adding protein inhibitors, the Papp value was increased and oral absorption was improved. By studying the effects of different concentrations and different protein inhibitors on paeonol and Pae-Lips, it was showed that the absorption mechanism of paeonol was passive transport, involving the participation of three efflux proteins, which was consistent with the experimental results of the Caco-2 monolayer cell model. Therefore, the in vitro cell experiments and in vivo intestinal absorption experiments further confirmed that the absorption mechanism of paeonol was passive transport and involved the participation of P-gp, MRP2 and BCRP efflux proteins, which was consistent with the reported literature.[46]

According to reports, paeonol has anti-inflammatory effects.[47,48] In this paper, LPS stimulated RAW264.7 macrophages were used to study the anti-inflammatory effects of paeonol and Pae-Liposomes. Macrophages are heterogeneous, the stimulation of LPS will cause the cell polarization to be classically activated (M1).[49] M1 type macrophages mainly secrete pro-inflammatory factors to promote the development of inflammatory response.[50] After paeonol and Pae-Lips protection, compared with the LPS group, the oxidative stress product NO and inflammatory factors IL-6, TNF-α in the supernatant of RAW264.7 were decreased in a concentration-dependent manner. Conversely, the level of the anti-inflammatory factor IL-10 was elevated. These results proved that paeonol and Pae-Lips have a good inhibitory effect on the M1 polarization of RAW264.7 macrophages. The inhibitory effect was: Pae-Lips-H > Pae-Lips-M > paeonol > Pae-Lips-L. These results showed that liposomes significantly enhanced the anti-inflammatory effect of paeonol.

DSS-induced ulcerative colitis in mice is the most common experimental model and is widely used because it is similar to human UC in morphology, pathophysiology and cytokines.[51] Therefore, this paper used the DSS-induced mouse UC model to evaluate the therapeutic efficacy of paeonol and Pae-Lips on UC. The experimental results found that compared with the model group, the DAI of the drug treatment groups were significantly reduced, the length of the colon was increased, and the inflammation observed by histopathology was significantly improved, confirming that paeonol and Pae-Lips significantly improved the UC process. Next, we studied the effect of drug treatment on inflammatory factors. IL-6 and TNF-α are recognized pro-inflammatory factors that mediate UC,[52,53] IL-10 is an anti-inflammatory factor that plays a major role in inhibiting the release of inflammatory factors and inflammatory response, regulating the differentiation of diverse immune cells.[54,55] The results of the Elisa kit showed that compared with the DSS group, the levels of IL-6 and TNF-α in the drug treatment groups were significantly reduced, and the level of IL-10 was increased, which once again demonstrated the anti-UC effects of paeonol and Pae-Lips. In order to further study the possible anti-inflammatory molecular mechanism, the expression of related proteins was determined by immunohistochemistry. Previous studies have shown that NF-κB and MAPK were the two main signal pathways that mediated the inflammatory response.[56–58] NF-κB comprises a family of inducible transcription factors that serve as important regulators of the inflammatory response.[59] p38 MAPK is one of the key MAPK signals, and recent research results indicate that the p38 MAPK signaling pathway was activated during the development of UC.[60,61] Therefore, p38 and NF-κB were chosen to measure protein expression. The experimental results found that the drug treatment group significantly inhibited the protein phosphorylation of p38 and NF-κB in the DSS-induced UC model and reduced protein expression, indicating that paeonol and Pae-Lips might inhibit the production of inflammatory factors by blocking the NF-κB and MAPK pathways, which is consistent with previous reports.[62–64] In short, in the anti-DSS-induced mouse UC experiment, paeonol and Pae-Lips have superior effects, and all anti-UC results are shown as: SASP > Pae-Lips-H > Pae-Lips-M > Paeonol > Pae-Lips-L. Compared with the paeonol group, the liposome groups have significantly enhanced anti-UC effect.

Conclusion

In this paper, paeonol liposomes were successfully prepared, and their quality was evaluated. The absorption mechanism of liposomes was investigated through in vivo pharmacokinetic experiments, in situ single-pass intestinal perfusion in rats and Caco-2 cell monolayer model. The liposome improves the bioavailability of paeonol and promotes the absorption of paeonol in the body. The absorption mode of paeonol is passive transport, and it is the substrate of P-gp, MRP2 and BCRP. Through in vitro and in vivo anti-inflammatory experiments, it was found that the anti-

inflammatory effect of drug-loaded liposomes was significantly better than that of paeonol suspension, which provided an experimental basis for further development of paeonol liposomes.

Acknowledgments

This work was supported by Subject Innovation Team of Shaanxi University of Chinese Medicine (NO. 2019-YL11), Scientific Research Project of Education Department of Shaanxi Provincial Government (NO. 21JS009).

Disclosure

The authors report no conflicts of interest in this work.

References

1. Pan. X, Wang H, Zheng Z, et al. Pectic polysaccharide from Smilax China L. ameliorated ulcerative colitis by inhibiting the galectin- 3/NLRP3 inflammasome pathway. *Carbohydr Polym*. 2022;277:118864. doi:10.1016/j.carbpol.2021.118864
2. Guan Q. A comprehensive review and update on the pathogenesis of inflammatory bowel disease. *J Immunol Res*. 2019;2019:7247238. doi:10.1155/2019/7247238
3. Zheng. JD, He Y, Yu. HY, et al. Unconjugated bilirubin alleviates experimental ulcerative colitis by regulating intestinal barrier fu nction and immune inflammation. *World J Gastroenterol*. 2019;25(15):1865–1878. doi:10.3748/wjg.v25.i15.1865
4. Rezaie A, Parker RD, Abdollahi M. Oxidative stress and pathogenesis of inflammatory bowel disease: an epiphenomenon or the cause? *Dig Dis Sci*. 2007;52(9):2015–2021. doi:10.1007/s10620-006-9622-2.
5. Feuerstein JD, Cheifetz AS. Ulcerative colitis: epidemiology. diagnosis. and management. *Mayo Clin Proc*. 2014;89(11):1553–1563. doi:10.1016/j.mayocp.2014.07.002.
6. Jain. S, Ahuja V, Limdi JK. Optimal management of acute severe ulcerative colitis. *Postgrad Med J*. 2019;95(1119):32–40. doi:10.1136/postgradmedj-2018-136072.
7. Gu LM, Li H, Xia JQ, et al. Huangqin decoction attenuates DSS-induced mucosal damage and promotes epithelial repair via inhibitin g TNF-¦Á-Induced NF-¦ÊB activation. *Chin J Integr Med*. 2021. doi:10.1007/s11655-021-3343-4.
8. Yuan. Z, Yang L, Zhang X, et al. Mechanism of Huang-lian-Jie-du decoction and its effective fraction in alleviating acute ulcerative c olitis in mice: regulating arachidonic acid metabolism and glycerophospholipid metabolism. *J Ethnopharmacol*. 2020;259:112872. doi:10.1016/j.jep.2020.112872.
9. Zhou C, Zhou H, Zhang F, et al. Active ingredients and potential mechanisms of the Gan Jiang-Huang Qin-Huang Lian-Ren Shen decoction against ulcerative colitis: a network pharmacology and molecular docking-based study. *Evid Based Complement Alternat Med*. 2021;2021:1925718. doi:10.1155/2021/1925718.
10. Wang Z, He C, Peng Y, et al. Origins. phytochemistry. pharmacology. analytical methods and safety of cortex moutan (Paeonia suffru ticosa Andrew): a systematic review. *Molecules*. 2017;22(6). doi:10.3390/molecules22060946.
11. Miao. J, Zhong J, Lan J, et al. Paeonol attenuates inflammation by confining HMGB1 to the nucleus. *J Cell Mol Med*. 2021;25(6):2885–2899. doi:10.1111/jcmm.16319
12. Qian. W, Li X, Yang M, et al. Antibacterial and anti-biofilm activities of paeonol against Klebsiella pneumoniae and Enterobacter cloacae. *Biofouling*. 2021;37(6):666–679. doi:10.1080/08927014.2021.1955249
13. Kim. SH, Kim SA, Park MK, et al. Paeonol inhibits anaphylactic reaction by regulating histamine and TNF-alpha. *Int Immunopharmacol*. 2004;4(2):279–287. doi:10.1016/j.intimp.2003.12.013
14. Liu LH, Shi. RJ, Chen ZC. Paeonol exerts anti?tumor activity against colorectal cancer cells by inducing G0/G1 phase arrest and cell apoptosis via inhibiting the Wnt/¦Â?catenin signaling pathway. *Int J Mol Med*. 2020;46(2):675–684. doi:10.3892/ijmm.2020.4629
15. Qi JH, Dong. FX, Wang XL. Exploring targets and signaling pathways of paeonol involved in relieving inflammation based on moder n technology. *Mol Divers*. 2021. doi:10.1007/s11030-021-10301-8
16. Himaya. SW, Ryu B, Qian. ZJ, et al. Paeonol from Hippocampus kuda Bleeler suppressed the neuro-inflammatory responses in vitro via NF-¦ÊB and MAPK signaling pathways. *Toxicol In Vitro*. 2012;26(6):878–887. doi:10.1016/j.tiv.2012.04.022
17. Jin. X, Wang J, Xia. ZM, et al. Anti-inflammatory and anti-oxidative activities of paeonol and its metabolites through blocking MAPK/ ERK/p38 signaling pathway. *Inflammation*. 2016;39(1):434–446. doi:10.1007/s10753-015-0265-3
18. Adki KM, Kulkarni YA. Chemistry. pharmacokinetics. pharmacology and recent novel drug delivery systems of paeonol. *Life Sci*. 2020;250:117544. doi:10.1016/j.lfs.2020.117544
19. Hu. X, Ding L, Cao S, et al. Pharmacokinetics. tissue distribution and excretion of paeonol and its major metabolites in rats prov ide a further insight into paeonol effectiveness. *Front Pharmacol*. 2020;11:190. doi:10.3389/fphar.2020.00190
20. Wang. F, Shan Q, Chang X, et al. Paeonol-loaded PLGA nanoparticles as an oral drug delivery system: design. optimization and evaluation. *Int J Pharm*. 2021;602:120617. doi:10.1016/j.ijpharm.2021
21. Yao. J, Zhang Y, Hu Q, et al. Optimization of paeonol-loaded poly(butyl-2-cyanoacrylate) nanocapsules by central composite design with response surface methodology together with the antibacterial properties. *Eur J Pharm Sci*. 2017;101:189–199. doi:10.1016/j.ejps.2017.01.028
22. Sheoran. R, Khokra SL, Chawla. V, et al. Recent patents. formulation techniques. classification and characterization of liposomes. *Recent Pat Nanotechnol*. 2019;13(1):17–27. doi:10.2174/1872210513666181127110413
23. Guimarães D, Cavaco-Paulo A. Design of liposomes as drug delivery system for therapeutic applications. *Int J Pharm*. 2021;601:120571. doi:10.1016/j.ijpharm.2021.120571
24. Li M, Du C, Guo N, et al. Composition design and medical application of liposomes. *Eur J Med Chem*. 2019;164:640–653. doi:10.1016/j.ejmech.2019.01.007

25. Catalan-Latorre. A, Ravaghi M, Manca M, et al. Freeze-dried eudragit-hyaluronan multicompartment liposomes to improve the intestinal bioavailability of curcumin. *Eur j Pharma Biopharma*. 2016;107:49–55. doi:10.1016/j.ejpb.2016.06.016
26. Manconi. M, Nácher A, Merino V, et al. Improving oral bioavailability and pharmacokinetics of liposomal metformin by glycerolphosphate-chitosan microcomplexation. *AAPS PharmSciTech*. 2013;14(2):485–496. doi:10.1208/s12249-013-9926-4
27. Liu. Y, Sun C, Li W, et al. Preparation and characterization of syringic acid-loaded TPGS liposome with enhanced oral bioavailabi lity and in vivo antioxidant efficiency. *AAPS PharmSciTech*. 2019;20(3):98. doi:10.1208/s12249-019-1290-6
28. Miao. Z, Zhang L, Gu M, et al. Preparation of fraxetin long circulating liposome and its anti-enteritis effect. *AAPS PharmSciTech*. 2021;22(3):110. doi:10.1208/s12249-021-01940-z
29. Wang. Q, Wei C, Weng W, et al. Enhancement of oral bioavailability and hypoglycemic activity of liquiritin-loaded precursor liposome. *Int J Pharm*. 2021;592:120036. doi:10.1016/j.ijpharm.2020.120036
30. Ge. Y, Pan M, Zhang C, et al. Paeonol alleviates dextran sodium sulfate induced colitis involving Candida albicans-associated dysbi osis. *Med Mycol*. 2021;59(4):335–344. doi:10.1093/mmy/myaa053
31. Zhang. L, Li DC, Liu LF. Paeonol: pharmacological effects and mechanisms of action. *Int Immunopharmacol*. 2019;72:413–421. doi:10.1016/j.intimp.2019.04.033
32. Tu. Y, Li L, Wang Z, et al. Advances in analytical techniques and quality control of traditional Chinese medicine injections. *J Pharm Biomed Anal*. 2021;206:114353. doi:10.1016/j.jpba.2021.114353
33. Chen. S, Zhang J, Wu L, et al. Paeonol nanoemulsion for enhanced oral bioavailability: optimization and mechanism. *Nanomedicine*. 2018;13(3):269–282. doi:10.2217/nnm-2017-0277
34. Li. H, Zhu J, Wang C, et al. Paeonol loaded cyclodextrin metal-organic framework particles for treatment of acute lung injury via inhalation. *Int J Pharm*. 2020;587:119649. doi:10.1016/j.ijpharm.2020.119649
35. Nunna. S, Huang YP, Rasa M, et al. Characterization of novel alpha-Mangostin and Paeonol derivatives with cancer-selective cytotoxicity. *Mol Cancer Ther*. 2021;21:257–270. doi:10.1158/1535-7163.mct-20-0787
36. Martí Coma-Cros. E, Biosca A, Lantero E, et al. Antimalarial activity of orally administered curcumin incorporated in eudragit-containing liposomes. *Int J Mol Sci*. 2018;19(5):1361. doi:10.3390/ijms19051361
37. Pires. CL, Praça C, Martins. PAT, et al. Re-use of Caco-2 monolayers in permeability assays-validation regarding cell monolayer integrity. *Pharmaceutics*. 2021;13(10):1563. doi:10.3390/pharmaceutics13101563
38. Chanez-Paredes. SD, Abtahi S, Kuo. WT, et al. Differentiating between tight junction-dependent and tight junction-independent intestinal barrier lo ss in vivo. *Methods Mol Biol*. 2021;2367:249–271. doi:10.1007/7651_2021_389
39. Sodhi JK, Benet LZ. The necessity of using changes in absorption time to implicate intestinal transporter involvement in oral drug-drug interactions. *Aaps J*. 2020;22(5):111. doi:10.1208/s12248-020-00469-6
40. Domínguez CJ, Tocchetti GN, Rigalli. JP, et al. Acute regulation of apical ABC transporters in the gut. Potential influence on drug bioavailability. *Pharmacol Res*. 2021;163:105251. doi:10.1016/j.phrs.2020.105251
41. Liu X. ABC Family Transporters. *Adv Exp Med Biol*. 2019;1141:13–100. doi:10.1007/978-981-13-7647-4_2
42. Drozdzik. M, Busch D, Lapczuk J, et al. Protein abundance of clinically relevant drug transporters in the human liver and intestine: a compar ative analysis in paired tissue specimens. *Clin Pharmacol Ther*. 2019;105(5):1204–1212. doi:10.1002/cpt.1301
43. He. ZX, Zhao TQ, Gong. YP, et al. Pyrimidine: a promising scaffold for optimization to develop the inhibitors of ABC transporters. *Eur J Med Chem*. 2020;200:112458. doi:10.1016/j.ejmech.2020.112458
44. Toyoda. Y, Takada T, Suzuki H. Inhibitors of human ABCG2: from technical background to recent updates with clinical implications. *Front Pharmacol*. 2019;10:208. doi:10.3389/fphar.2019.00208
45. Babadi. D, Dadashzadeh S, Osouli M, et al. Nanoformulation strategies for improving intestinal permeability of drugs: a more precise look at per meability assessment methods and pharmacokinetic properties changes. *J Control Release*. 2020;321:669–709. doi:10.1016/j.jconrel.2020.02.041
46. Xu. Y, Shrestha N, Pr¨¦at V, et al. Overcoming the intestinal barrier: a look into targeting approaches for improved oral drug delivery s ystems. *J Control Release*. 2020;322:486–508. doi:10.1016/j.jconrel.2020.04.006
47. Dahlgren. D, Roos C, Peters K, et al. Evaluation of drug permeability calculation based on luminal disappearance and plasma appearance in t he rat single-pass intestinal perfusion model. *Eur J Pharm Biopharm*. 2019;142:31–37. doi:10.1016/j.ejpb.2019.06.011
48. Ouyang Y, Zhang J, Dai HWM. Absorption mechanism of paeonol nanoemulsion using in vitro intestinal cell models. *J Chin Pharmaceut Sci*. 2019;28(03):174–185. doi:10.5246/jcps.2019.03.017
49. Liu. Y, Li C, Wu H, et al. Paeonol attenuated inflammatory response of endothelial cells via stimulating monocytes-derived exoso mal MicroRNA-223. *Front Pharmacol*. 2018;9:1105. doi:10.3389/fphar.2018.01105
50. Qiu. C, Yang LD, Yu W, et al. Paeonol ameliorates CFA-induced inflammatory pain by inhibiting HMGB1/TLR4/NF-¦ÊB p65 pathway. *Metab Brain Dis*. 2021;36(2):273–283. doi:10.1007/s11011-020-00645-9
51. Shapouri-Moghaddam. A, Mohammadian S, Vazini H, et al. Macrophage plasticity. polarization. and function in health and disease. *J Cell Physiol*. 2018;233(9):6425–6440. doi:10.1002/jcp.26429
52. Liu. YC, Zou XB, Chai. YF, et al. Macrophage polarization in inflammatory diseases. *Int J Biol Sci*. 2014;10(5):520–529. doi:10.7150/ijbs.8879
53. Eichele DD, Kharbanda KK. Dextran sodium sulfate colitis murine model: an indispensable tool for advancing our understanding of inflammatory bowel diseases pathogenesis. *World J Gastroenterol*. 2017;23(33):6016–6029. doi:10.3748/wjg.v23.i33.6016
54. Tatiya-Aphiradee. N, Chatuphonprasert W, Jarukamjorn K. Immune response and inflammatory pathway of ulcerative colitis. *J Basic Clin Physiol Pharmacol*. 2018;30(1):1–10. doi:10.1515/jbcpp-2018-0036
55. Wang. C, Li W, Wang H, et al. Saccharomyces boulardii alleviates ulcerative colitis carcinogenesis in mice by reducing TNF-¦Á and IL −6 levels and functions and by rebalancing intestinal microbiota. *BMC Microbiol*. 2019;19(1):246. doi:10.1186/s12866-019-1610-8
56. Papoutsopoulou. S, Pollock L, Walker C, et al. Impact of Interleukin 10 deficiency on intestinal epithelium responses to inflammatory signals. *Front Immunol*. 2021;12:690817. doi:10.3389/fimmu.2021.690817
57. Sun. X, Huang Y, Zhang. YL, et al. Research advances of vasoactive intestinal peptide in the pathogenesis of ulcerative colitis by regul ating interleukin-10 expression in regulatory B cells. *World J Gastroenterol*. 2020;26(48):7593–7602. doi:10.3748/wjg.v26.i48.7593
58. Ma. H, Zhou M, Duan W, et al. Anemoside B4 prevents acute ulcerative colitis through inhibiting of TLR4/NF-¦ÊB/MAPK signaling pathway. *Int Immunopharmacol*. 2020;87:106794. doi:10.1016/j.intimp.2020.106794

59. Wei. YY, Fan YM, Ga Y, et al. Shaoyao decoction attenuates DSS-induced ulcerative colitis. macrophage and NLRP3 inflammasome activa tion through the MKP1/NF-¦ÊB pathway. *Phytomedicine*. 2021;92:153743. doi:10.1016/j.phymed.2021.153743
60. Zobeiri. M, Momtaz S, Parvizi F, et al. Targeting mitogen-activated protein kinases by natural products: a novel therapeutic approach for inf lammatory bowel diseases. *Curr Pharm Biotechnol*. 2020;21(13):1342–1353. doi:10.2174/1389201021666191216122555
61. Zaidi D, Wine E. Regulation of nuclear factor kappa-light-chain-enhancer of activated B Cells (NF-¦Ê¦Â) in inflammatory bowel diseases. *Front Pediatr*. 2018;6:317. doi:10.3389/fped.2018.00317
62. Almeer. RS, Mahmoud SM, Amin. HK, et al. Ziziphus spina-christi fruit extract suppresses oxidative stress and p38 MAPK expression in ulcerative colitis in rats via induction of Nrf2 and HO-1 expression. *Food Chem Toxicol*. 2018;115:49–62. doi:10.1016/j.fct.2018.03.002
63. Jia. L, Xue K, Liu J, et al. Anticolitic effect of berberine in rat experimental model: impact of PGE2/p38 MAPK pathways. *Mediators Inflamm*. 2020;2020:9419085. doi:10.1155/2020/9419085
64. Ishiguro. K, Ando T, Maeda O, et al. Paeonol attenuates TNBS-induced colitis by inhibiting NF-kappaB and STAT1 transactivation. *Toxicol Appl Pharmacol*. 2006;217(1):35–42. doi:10.1016/j.taap.2006.07.002